Journal of Coordination Chemistry

ISSN: 0095-8972 (Print) 1029-0389 (Online) Journal homepage: http://www.tandfonline.com/loi/gcoo20

Gadolinium(III) and dysprosium(III) complexes with a Schiff base bis(N-salicylidene)-3-oxapentane-1,5-diamine: synthesis, characterization, antioxidation, and DNA-binding studies

Chengyong Chen, Jiawen Zhang, Yanhui Zhang, Zaihui Yang, Huilu Wu, Guolong Pan & Yuchen Bai

To cite this article: Chengyong Chen, Jiawen Zhang, Yanhui Zhang, Zaihui Yang, Huilu Wu, Guolong Pan & Yuchen Bai (2015) Gadolinium(III) and dysprosium(III) complexes with a Schiff base bis(N-salicylidene)-3-oxapentane-1,5-diamine: synthesis, characterization, antioxidation, and DNA-binding studies, Journal of Coordination Chemistry, 68:6, 1054-1071, DOI: 10.1080/00958972.2015.1007965

To link to this article: http://dx.doi.org/10.1080/00958972.2015.1007965

Accepted author version posted online: 14 Jan 2015.
Published online: 09 Feb 2015.

Journal of Coordination Chemistry, 2015
Vol. 68, No. 6, 1054–1071, http://dx.doi.org/10.1080/00958972.2015.1007965

Gadolinium(III) and dysprosium(III) complexes with a Schiff base bis(*N*-salicylidene)-3-oxapentane-1,5-diamine: synthesis, characterization, antioxidation, and DNA-binding studies

CHENGYONG CHEN, JIAWEN ZHANG, YANHUI ZHANG, ZAIHUI YANG, HUILU WU*, GUOLONG PAN and YUCHEN BAI

School of Chemical and Biological Engineering, Lanzhou Jiaotong University, Lanzhou, PR China

(*Received 11 September 2014; accepted 29 December 2014*)

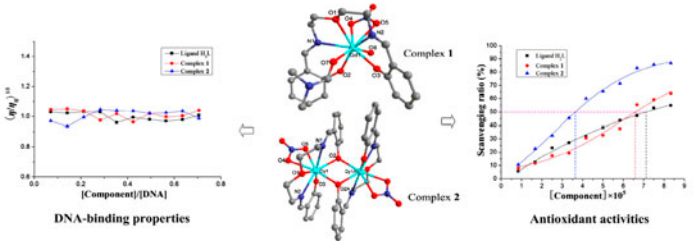

A pentadentate Schiff base bis(*N*-salicylidene)-3-oxapentane-1,5-diamine (H_2L) and its lanthanide (III) complexes, $[GdL(NO_3)(DMF)(H_2O)]$ (**1**) and $[Dy_2L_2(NO_3)_2]\cdot 2H_2O$ (**2**), have been synthesized and characterized by physical, chemical, and spectroscopic methods. Single crystal X-ray structure reveals that **1** is a discrete mononuclear species with nine-coordinate Gd(III) in a distorted mono-capped square antiprism geometry. Complex **2** is a centrosymmetric binuclear neutral entity, in which Dy(III) is eight-coordinate in a distorted square antiprism. Electronic absorption titration spectra, ethidium bromide competitive experiments, and viscosity measurements indicate that both the ligand and complexes bind calf thymus DNA, presumably via groove binding. Investigations of antioxidant activities show that both complexes have some scavenging effects for hydroxyl and superoxide radicals.

Keywords: Bis(*N*-salicylidene)-3-oxapentane-1,5-diamine; Lanthanide(III) complex; Crystal structure; DNA-binding property; Antioxidant activity

1. Introduction

During the past two decades, binding of transition metal complexes to DNA has been extensively studied [1–5] for gaining insight into the reactive models for protein–nucleic acid interactions and probes of DNA structure, and also for obtaining information about

*Corresponding author. Email: wuhl@mail.lzjtu.cn

drug design [6, 7]. Some metal complexes are being used to bind and react at specific sequences of DNA in a search for new chemotherapeutics, for probing DNA, and for the development of highly sensitive diagnostic agents [8, 9]. Basically, complexes bind to DNA through three non-covalent modes: intercalation, groove binding, and external static electronic effects [10–13]. The results may allow design of new compounds which can recognize specific sites or conformations of DNA [8, 9, 14].

Schiff bases are a very important class of compounds because of their ability to form stable complexes with many different transition and rare-earth metal ions in various oxidation states [15–18]. Chelation of metal ions by Schiff-base macrocycles (coronands) and open-chain (podands) ligands is of interest for the role played by these structures in bioinorganic and medicinal inorganic chemistry [19, 20]. Lanthanide metal complexes also have been used as biological models to understand the structures of biomolecules and biological processes [21–23]. One of the most studied applications is usage of lanthanide complexes to interact with DNA/RNA by non-covalent binding and/or cleavage [24–26].

Continuing our program for constructing Schiff-base ligands with rare-earth metal complexes, we have investigated the DNA binding ability of such complexes [27, 28]. In this article, we introduce the synthesis and structural characterization of two new lanthanide(III) complexes with a Schiff-base ligand bis(*N*-salicylidene)-3-oxapentane-1,5-diamine. The prepared pentadentate ligand contains strong donors, phenoxo oxygens, and imine nitrogens bearing excellent coordination ability with metal ions through its N_2O_3 donor set. The DNA binding properties of the complexes were investigated by spectrophotometric and viscosity measurements. In addition, the antioxidant activities of the complexes were determined by the superoxide anion ($O_2^{-\cdot}$) and hydroxyl radical (OH·) scavenging methods *in vitro*.

2. Experimental

2.1. *Materials and methods*

C, H, and N elemental analyses were determined using a Carlo Erba 1106 elemental analyzer. The water content was determined by thermogravimetric analysis (TGA). Thermal analyses were carried out under N_2 flow at a heating rate of 10 °C min^{-1} on a ZRY-2P thermal analyzer. ^{1}H NMR spectra were obtained with a Mercury plus 400 MHz NMR spectrometer with TMS as internal standard and $CDCl_3$ as solvent. IR spectra were recorded from 4000 to 400 cm^{-1} with a Nicolet FT-VERTEX 70 spectrometer using KBr pellets. Electronic spectra were taken on Lab-Tech UV Bluestar and Spectrumlab 722sp spectrophotometers and the spectral resolution used is 0.2 nm. Fluorescence spectra were recorded on a LS-45 spectrofluorophotometer.

All chemicals were of analytical grade. Calf thymus DNA (CT-DNA), ethidium bromide (EB), nitroblue tetrazolium nitrate (NBT), methionine (MET), and riboflavin ($VitB_2$) were obtained from Sigma–Aldrich Co. (USA) and used without purification. The stock solution of complex was dissolved in DMF at 3×10^{-3} M. The solution of CT-DNA gave a ratio of UV absorbances at 260 and 280 nm, A_{260}/A_{280}, of 1.8–1.9, indicating that the DNA was sufficiently free of protein [29]. The stock solution of DNA (2.5×10^{-3} M) was prepared in 5 mM Tris–HCl/50 mM NaCl buffer solution (pH 7.2, stored at 4 °C and used after not

more than four days). The CT-DNA concentration per nucleotide was determined spectrophotometrically by employing an extinction coefficient of 6600 M^{-1} cm^{-1} at 260 nm [30].

2.2. *Synthesis*

2.2.1. Preparation of 3-oxapentane-1,5-diamine. 3-Oxapentane-1,5-diamine was synthesized following the procedure [31]. Found (%): C, 45.98; H, 11.50; N, 26.76. Calcd (%) for $C_4H_{12}N_2O$: C, 46.25; H, 11.54; N, 26.90. FT-IR (KBr ν/cm^{-1}): 1120, ν_{as}(C–O–C); 3340, ν(–NH_2) stretching frequency, respectively.

2.2.2. Bis(*N*-salicylidene)-3-oxapentane-1,5-diamine (H_2L). The synthesis of H_2L was similar to that reported by Wu *et al.* [32]. Found (%): C, 69.09; H, 6.54; N, 8.83. Calcd (%) for $C_{18}H_{20}O_3N_2$: C, 69.21; H, 6.45; N, 8.97. ^{1}H–NMR ($CDCl_3$, 400 MHz) δ/ppm: 13.49 (s, 2H, Ar–OH), 8.30 (s, 2H, N=CH), 6.79–7.33 (m, 8H, H-benzene ring), 3.66–3.74 (m, 8H, O–$(CH_2)_2$–N=C). UV–vis (λ, nm): 268, 316. FT-IR (KBr, ν/cm^{-1}): 1637, ν(C=N); 1286, ν_{as}(C–O–C); 3458, ν(OH) stretching frequency, respectively. The synthetic route is in scheme 1.

2.2.3. Synthesis of [GdL(NO_3)(DMF)(H_2O)] (1). To a stirred solution of H_2L (0.156 g, 0.5 mM) in EtOH (10 mL) was added $Gd(NO_3)_3(H_2O)_6$ (0.226 g, 0.5 mM) and triethylamine (0.3 mL) in EtOH (10 mL). The yellow sediment appeared rapidly. The precipitate was filtered off, washed with EtOH and absolute Et_2O, and dried *in vacuo*. The dried precipitate was dissolved in DMF to form a yellow solution. Yellow block crystals of **1** suitable for X-ray diffraction studies were obtained by vapor diffusion of diethyl ether into the solution for a few weeks at room temperature. Yield: 0.197 g (51.6%). Found (%): C, 40.33; H, 4.72; N, 8.87. Calcd (%) for $C_{21}H_{27}N_4O_8Gd$: C, 40.64; H, 4.38; N, 9.03. UV–vis (λ, nm): 268, 316. FT-IR (KBr, ν/cm^{-1}): 1274, ν_{as}(C–O–C); 1341, 1052, ν(NO_3); 1628, ν(C=N).

2.2.4. Synthesis of [$Dy_2L_2(NO_3)_2$]·$2H_2O$ (2). **2** was obtained by a similar procedure to that used for preparation of **1** except for using $Dy(NO_3)_3(H_2O)_6$ (0.228 g, 0.5 mM) instead of $Gd(NO_3)_3(H_2O)_6$. Yield: 0.211 g (54.9%). Found (%): C, 39.46; H, 3.43; N, 7.32. Calcd (%) for $C_{36}H_{40}Dy_2N_6O_{14}$: C, 39.10; H, 3.65; N, 7.61. UV–vis (λ, nm): 269, 316. FT-IR (KBr, ν/cm^{-1}): 1271, ν_{as}(C–O–C); 1382, 1029, ν(NO_3); 1629, ν(C=N).

2.3. *X-ray crystallography*

A suitable single crystal was mounted on a glass fiber, and the intensity data were collected on a Bruker Smart CCD diffractometer with graphite-monochromated Mo-Kα radiation (λ = 0.71073 Å) at 296 K. Data reduction and cell refinement were performed using SMART and SAINT programs [33]. The structure was solved by direct methods and refined by full-matrix least-squares against F^2 of data using SHELXTL software [34]. The uncoordinated water was disordered. Its electron density was removed from the reflection intensities by using the routine SQUEEZE in PLATON. All hydrogens were found in difference

electron maps and subsequently refined in a riding-model approximation with C–H distances ranging from 0.93 to 0.97 Å and $U_{iso}(H) = 1.2\ U_{eq}(C)$ or $1.5\ U_{eq}(C)$. The unit cell of **2** contains disordered water molecules which have been treated as a diffuse contribution to the overall scattering without specific atom positions by SQUEEZE/PLATON.

2.4. *DNA-binding experiments*

2.4.1. Electronic absorption titration. Absorption titration experiments were performed with fixed concentrations of the complexes, while gradually increasing the concentration of CT-DNA. To obtain absorption spectra, the required amount of CT-DNA was added to both the compound and reference solutions, in order to eliminate the absorbance of CT-DNA itself. From the absorption titration data, the binding constant (K_b) was determined using [35]:

$$[\mathrm{DNA}]/(\varepsilon_a - \varepsilon_f) = [\mathrm{DNA}]/(\varepsilon_b - \varepsilon_f) + 1/K_b(\varepsilon_b - \varepsilon_f)$$

where [DNA] is the concentration of CT-DNA in base pairs, ε_a corresponds to the observed extinction coefficient (A_{obsd}/[M]), ε_f corresponds to the extinction coefficient of the free compound, ε_b is the extinction coefficient of the compound when fully bound to CT-DNA, and K_b is the intrinsic binding constant. The ratio of slope to intercept in the plot of $[\mathrm{DNA}]/(\varepsilon_a - \varepsilon_f)$ *versus* [DNA] gave the value of K_b.

2.4.2. Fluorescence studies. The enhanced fluorescence of EB in the presence of DNA can be quenched by the addition of another binder [36, 37]. The extent of fluorescence quenching of EB bound to CT-DNA can be used to determine the extent of binding between the second molecule and CT-DNA. Competitive binding experiments were carried out in the buffer by keeping [DNA]/[EB] = 1 and varying the concentrations of the compounds. The fluorescence spectra of EB were measured using an excitation wavelength of 520 nm, and the emission range was set between 550 and 750 nm. The spectra were analyzed according to the classical Stern–Volmer equation [38]:

$$I_0/I = 1 + K_{SV}[Q]$$

where I_0 and I are the fluorescence intensities at 599 nm in the absence and presence of the quencher, respectively, K_{sv} is the linear Stern–Volmer quenching constant, and [Q] is the concentration of the quencher. In these experiments [CT-DNA] = 2.5×10^{-3} M/L, [EB] = 2.2×10^{-3} M/L.

2.4.3. Viscosity titration measurements. Viscosity experiments were conducted on an Ubbelohde viscometer, immersed in a water bath maintained at 25.0 ± 0.1 °C. The flow time was measured with a digital stopwatch and each sample was tested three times to get an average calculated time. Titrations were performed for the complexes (3–30 μM), and each compound was introduced into CT-DNA solution (42.5 μM) present in the viscometer. Data were analyzed as $(\eta/\eta_0)^{1/3}$*versus* the ratio of the concentration of the compound to CT-DNA, where η is the viscosity of CT-DNA in the presence of the compound and η_0 is

the viscosity of CT-DNA alone. Viscosity values were calculated from the observed flow time of CT-DNA-containing solutions corrected from the flow time of buffer alone (t_0), $\eta = (t - t_0)$ [39].

2.5. *Antioxidant study methods*

2.5.1. Hydroxyl radical assay. Hydroxyl radicals were generated in aqueous media through the Fenton-type reaction [40, 41]. Aliquots of reaction mixture (3 mL) contained 1 mL of 0.1 mM aqueous safranin, 1 mL of 1.0 mM aqueous EDTA–Fe(II), 1 mL of 3% aqueous H_2O_2, and a series of quantitative microadditions of solutions of the test compound. A sample without the tested compound was used as the control. The reaction mixtures were incubated at 37 °C for 30 min in a water bath. The absorbance was then measured at 520 nm. All the tests were run in triplicate and are expressed as the mean and standard deviation [42]. The scavenging effect for OH· was calculated from the following expression:

$$\text{Scavenging ratio } (\%) = [(A_i - A_0)/(A_c - A_0)] \times 100\%$$

where A_i – absorbance in the presence of the test compound; A_0 – absorbance of the blank in the absence of the test compound; A_c – absorbance in the absence of the test compound, EDTA–Fe(II) and H_2O_2.

2.5.2. Superoxide radical assay. A nonenzymatic system containing 1 mL 9.9×10^{-6} M VitB2, 1 mL 1.38×10^{-4} M NBT, and 1 mL 0.03 M MET was used to produce superoxide anion ($O_2^{-\cdot}$), and the scavenging rate of $O_2^{-\cdot}$ under the influence of 0.1–1.0 μM tested compound was determined by monitoring the reduction in rate of transformation of NBT to monoformazan dye [43]. The solution of MET, VitB2, and NBT was prepared with 0.02 M phosphate buffer (pH 7.8) avoiding light. The reactions were monitored at 560 nm with a UV–vis spectrophotometer, and the rate of absorption change was determined. The percentage inhibition of NBT reduction was calculated using the equation [44]:

$$\text{Percentage inhibition of NBT reduction} = (1 - k'/k) \times 100$$

where k' and k present the slopes of the straight line of absorbance values as a function of time in the presence and absence of SOD mimic compound (SOD is superoxide dismutase). The IC_{50} values for the complexes were determined by plotting the graph of percentage inhibition of NBT reduction against the increase in the concentration of the complex. The concentration of the complex which causes 50% inhibition of NBT reduction is reported as IC_{50}.

3. Results and discussion

The Ln(III) complexes, prepared by reaction of H_2L with $Ln(NO_3)_3(H_2O)_6$ in ethanol, are soluble in polar aprotic solvents such as DMF, DMSO, and MeCN, slightly soluble in ethanol, methanol, ethyl acetate, and chloroform and insoluble in water, Et_2O, and petroleum

ether. The elemental analyses show their composition which were confirmed by crystal structure analysis.

The TGA curves of **2** show that it undergoes endothermic dehydration. Mass losses from 85 to 110 °C are attributed to elimination of hydration H_2O molecules; DTA curves indicate that the dehydration process has an endothermic peak. The results indicate **2** has two water molecules.

3.1. *IR and electronic spectra*

The IR spectra of the Ln(III) complexes (Ln = Gd, Dy) were analyzed in comparison with that of free H_2L from 4000 to 400 cm^{-1}. In H_2L, a strong band is at 1637 cm^{-1} with a weak band at 1286 cm^{-1}. By analogy with the assigned bands, the former can be attributed to ν(C=N), while the latter can be attributed to the asymmetric stretch of C–O–C [45, 46]. The two bands are slightly shifted for **1**, the band at 1637–1628 cm^{-1} and the band at 1286–1274 cm^{-1}, which can be attributed to coordination of the ligand. Similar shifts also appear in **2** (1629, 1271 cm^{-1}), which give the same conclusion. Bands at 1341, 1052 cm^{-1} in **1** and 1382, 1029 cm^{-1} in **2** indicate bidentate nitrate [47], in agreement with X-ray diffraction.

DMF solutions of H_2L and Ln(III) complexes show almost identical UV spectra. The UV bands of H_2L (268, 316 nm) are marginally shifted in complexes, providing further evidence for nitrogen and oxygen coordination. Two absorptions are assigned to $\pi \rightarrow \pi^*$ (benzene) and $\pi \rightarrow \pi^*$(C=N) transitions [48].

Table 1. Crystal and structure refinement data for **1** and **2**.

Complex	$[GdL(NO_3)(DMF)(H_2O)]$ (**1**)	$[Dy_2L_2(NO_3)_2]\cdot 2H_2O$ (**2**)
Molecular formula	$C_{21}H_{27}GdN_4O_8$	$C_{36}H_{36}Dy_2N_6O_{12}$
Molecular weight	620.72	1069.71
Crystal size (mm)	0.26 × 0.24 × 0.20	0.26 × 0.23 × 0.20
Crystal system	Monoclinic	Monoclinic
Space group	$P2_1/n$	$C2/c$
a (Å)	11.509(2)	29.353(5)
b (Å)	12.019(2)	11.767(2)
c (Å)	18.398(4)	15.179(3)
α (°)	90	90
β (°)	106.400(2)	117.750(2)
γ (°)	90	90
V (Å^3)	2441.3(8)	4639.6(15)
Z	4	4
D_{calcd} (g cm^{-3})	1.689	1.531
F (000)	1236	2088
θ range for data collection (°)	2.31–25.50	2.65–25.50
$h/k/l$ (max, min)	−13,13/−13,14/−22,11	−32,35/−14,13/−18,15
Reflections collected	10,704	12,665
Independent reflections	4497 [R(int) = 0.0303]	4308 [R(int) = 0.0365]
Refinement method	Full-matrix least-squares on F^2	Full-matrix least-squares on F^2
Data/restraints/parameters	4497/3/309	4308/0/253
Reflections with $I > 2\sigma(I)$	3624	3161
Goodness-of-fit on F^2	1.028	0.987
Final R_1,wR_2 indices [$I > 2\sigma(I)$]	0.0283, 0.0544	0.0380, 0.0955
R_1,wR_2 indices (all data)	0.0409, 0.0586	0.0574, 0.1067
Largest diff. peak and hole (e Å^{-3})	0.604 and −0.364	2.402 and −0.802

3.2. *X-ray structures of the complexes*

Basic crystal data, description of the diffraction experiment, and details of the structure refinement are given in table 1. Selected bond distances and angles are presented in table 2.

Table 2. Selected bond distances (Å) and angles (°) in **1** and **2**.

Complex **1**			
Bond distances (Å)			
Gd(1)–O(3)	2.292(3)	Gd(1)–O(2)	2.320(3)
Gd(1)–O(8)	2.412(3)	Gd(1)–O(7)	2.415(3)
Gd(1)–O(5)	2.523(3)	Gd(1)–N(2)	2.566(3)
Gd(1)–N(1)	2.583(3)	Gd(1)–O(4)	2.584(3)
Gd(1)–O(1)	2.599(3)		
Bond angles (°)			
O(3)–Gd(1)–O(2)	82.00(9)	O(3)–Gd(1)–O(8)	75.74(9)
O(2)–Gd(1)–O(8)	72.91(9)	O(3)–Gd(1)–O(7)	81.96(10)
O(2)–Gd(1)–O(7)	79.35(9)	O(8)–Gd(1)–O(7)	146.35(9)
O(3)–Gd(1)–O(5)	97.05(9)	O(2)–Gd(1)–O(5)	140.27(9)
O(8)–Gd(1)–O(5)	68.48(9)	O(7)–Gd(1)–O(5)	140.14(9)
O(3)–Gd(1)–N(2)	71.07(10)	O(2)–Gd(1)–N(2)	144.37(10)
O(8)–Gd(1)–N(2)	120.11(9)	O(7)–Gd(1)–N(2)	74.25(9)
O(5)–Gd(1)–N(2)	67.96(9)	O(3)–Gd(1)–N(1)	145.79(10)
O(2)–Gd(1)–N(1)	69.51(9)	O(8)–Gd(1)–N(1)	111.64(10)
O(7)–Gd(1)–N(1)	74.67(10)	O(5)–Gd(1)–N(1)	116.91(10)
N(2)–Gd(1)–N(1)	123.90(10)	O(3)–Gd(1)–O(4)	137.60(9)
O(2)–Gd(1)–O(4)	107.00(9)	O(8)–Gd(1)–O(4)	68.21(9)
O(7)–Gd(1)–O(4)	140.02(9)	O(5)–Gd(1)–O(4)	49.52(9)
N(2)–Gd(1)–O(4)	108.61(10)	N(1)–Gd(1)–O(4)	71.28(10)
O(3)–Gd(1)–O(1)	133.37(9)	O(2)–Gd(1)–O(1)	131.29(8)
O(8)–Gd(1)–O(1)	137.71(8)	O(7)–Gd(1)–O(1)	75.56(9)
O(5)–Gd(1)–O(1)	76.79(9)	N(2)–Gd(1)–O(1)	63.74(9)
N(1)–Gd(1)–O(1)	63.92(9)	O(4)–Gd(1)–O(1)	71.07(9)
Complex **2**			
Bond distances (Å)			
Dy(1)–O(3)	2.173(4)	Dy(1)–O(2)#1[a]	2.291(3)
Dy(1)–O(2)	2.316(3)	Dy(1)–O(1)	2.468(4)
Dy(1)–O(4)	2.470(4)	Dy(1)–O(5)	2.480(4)
Dy(1)–N(2)	2.492(5)	Dy(1)–N(1)	2.505(5)
Bond angles (°)			
O(3)–Dy(1)–O(2)#1	95.74(15)	O(3)–Dy(1)–O(2)	86.27(14)
O(2)#1–Dy(1)–O(2)	70.90(13)	O(3)–Dy(1)–O(1)	140.28(14)
O(2)#1–Dy(1)–O(1)	87.38(13)	O(2)–Dy(1)–O(1)	131.33(13)
O(3)–Dy(1)–O(4)	96.49(18)	O(2)#1–Dy(1)–O(4)	157.31(14)
O(2)–Dy(1)–O(4)	128.95(15)	O(1)–Dy(1)–O(4)	71.07(15)
O(3)–Dy(1)–O(5)	83.16(16)	O(2)#1–Dy(1)–O(5)	150.10(12)
O(2)–Dy(1)–O(5)	79.22(12)	O(1)–Dy(1)–O(5)	112.47(14)
O(4)–Dy(1)–O(5)	50.89(14)	O(3)–Dy(1)–N(2)	74.17(17)
O(2)#1–Dy(1)–N(2)	85.03(14)	O(2)–Dy(1)–N(2)	147.30(15)
O(1)–Dy(1)–N(2)	66.66(17)	O(4)–Dy(1)–N(2)	80.03(16)
O(5)–Dy(1)–N(2)	122.75(15)	O(3)–Dy(1)–N(1)	152.70(16)
O(2)#1–Dy(1)–N(1)	89.82(14)	O(2)–Dy(1)–N(1)	70.32(14)
O(1)–Dy(1)–N(1)	66.51(14)	O(4)–Dy(1)–N(1)	88.03(19)
O(5)–Dy(1)–N(1)	78.92(15)	N(2)–Dy(1)–N(1)	133.05(17)

[a]Symmetry transformations used to generate equivalent atoms: #1 $-x + 1/2, -y + 3/2, -z$.

3.2.1. Crystal structure of 1. The crystal analysis reveals that **1** crystallizes in monoclinic space group *P*2(1)/*n*. The crystal structure of [GdL(NO_3)(DMF)(H_2O)] demonstrates a discrete mononuclear species with nine-coordinate GdN_2O_7 [two imine N(1) and N(2) from the amine part; one ether O(1); two coordinated phenoxo O(2) and O(3); O(7) from DMF; O(4) and O(5) from bidentate univalent NO_3^- and one coordinated water O(8)] as shown in figure 1(a). The coordination polyhedron around Gd(III) is a mono-capped square antiprism [figure 1(b)]. The bond lengths are Gd–$O_{phenoxo}$: 2.292(3)–2.320(3), Gd–O_{ether}: 2.599(3), Gd–O_{DMF}: 2.415(3), Gd–$O_{nitrate}$: 2.523(3)–2.584(3), and Gd–O_{water}: 2.412(3) Å, all of which are within the range of those observed for other nine-coordinate Ln(III) complexes with oxygen donor ligands [49–51].

Hydrogen-bonding interactions play important roles in crystal packing of **1** [45, 52]. As shown in figure 2, the neighboring [GdL(NO_3)(DMF)(H_2O)] moieties are connected by two hydrogen bonds between the metal coordinated H_2O and the ligand. The hydrogen bond details are presented in table 3 and an infinite 2-D layer is propagated due to the hydrogen-bonding interactions.

3.2.2. Crystal structure of 2. Complex **2** crystallizes in the monoclinic space group *C*2/*c* and crystallographic analysis reveals that **2** is a centrosymmetric neutral homobinuclear entity. The structure of **2** [figure 3(a)] shows two adjacent [DyL(NO_3)] moieties bridged via two phenoxo groups. In the μ_2-diphenoxo bridged binuclear structure, both Dy(III) centers are eight coordinate [figure 3(b)]. The solvent water is disordered so badly that it cannot be modeled even with restraints. Hence, we used PLATON/SQUEEZE routine to mask out the disordered density, affording approximately 568 $Å^3$ voids. The number of solvent water molecules was established by thermogravimetric method, and experimental result indicates

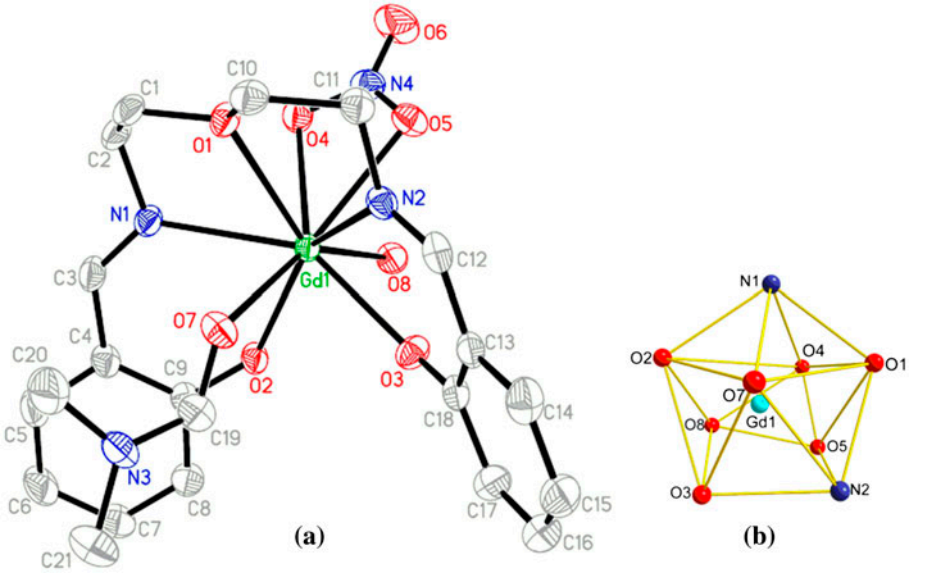

Figure 1. (a) The molecular structure of **1** in the crystal with displacement ellipsoids at 30% probability level; hydrogens are omitted for clarity. (b) Coordination polyhedron of Gd.

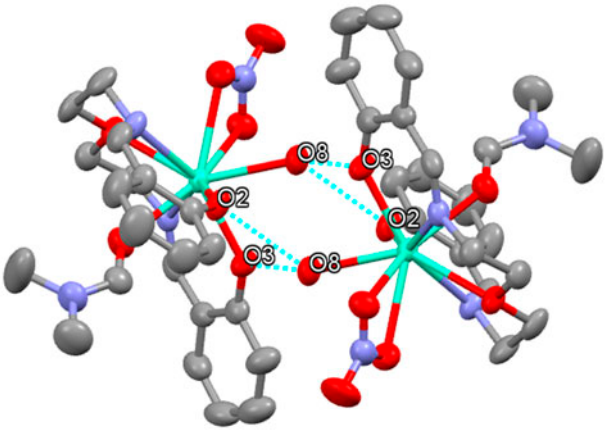

Figure 2. 2-D layer structure formed of **1** constructed by hydrogen bonds which are indicated with dashed green lines (see http://dx.doi.org/10.1080/00958972.2015.1007965 for color version).

the crystal structure of **2** consists of two water molecules. The local coordination environment is identical for both the centers by symmetry and is best described as a distorted DyN_2O_6 square antiprism [figure 3(b)]. Due to the flexibility of the ligand, it loses its planarity. The bond lengths are Dy(1)–N_{imine}: 2.492(5)–2.505(5), Dy(1)–O_{ether}: 2.468(4), and Dy(1)–$O_{nitrate}$: 2.470(4)–2.480(4) Å. The nature of coordination of the two identical Schiff-base moieties of the same ligand is completely different. Of the two phenoxo oxygens of each ligand, one is monocoordinated while the other bridges adjacent Dy(III) centers as reflected by the Dy–$O_{phenoxo}$ bond lengths [Dy(1)–O(2), 2.316(3) and Dy(1)–O(3), 2.173 (4) Å]. The Dy(1)–Dy(1A) distance of 3.7535(8) Å is too long to consider any direct intramolecular Dy–Dy interaction.

3.3. *DNA binding properties*

3.3.1. Absorption spectroscopic studies. Application of electronic absorption spectroscopy in DNA-binding studies is one of the most useful techniques [53]. To clarify the interaction between the compounds and DNA, the electronic absorption spectra of H_2L and both Ln(III) complexes in the absence and in the presence of CT-DNA (at a constant concentration of the compounds) were obtained (shown in figure 4). With increasing DNA concentrations, the absorption at 394 nm of H_2L has hypochromism of 32.4%; the absorption at 391 nm of **1** exhibits hypochromism of 73.1%; the absorption at 390 nm of **2** has

Table 3. Hydrogen bonding distances (Å) and angles (°) of **1**.

D–H···A	D–H	D···A	D···A	∠DHA
O8–H1 W···O2[a]	0.76	2.706(4)	2.01	151.7
O8–H2 W···O3[a]	0.88	2.726(4)	1.88	159.0

[a]Symmetry codes: $1 - x, -y, -z$.

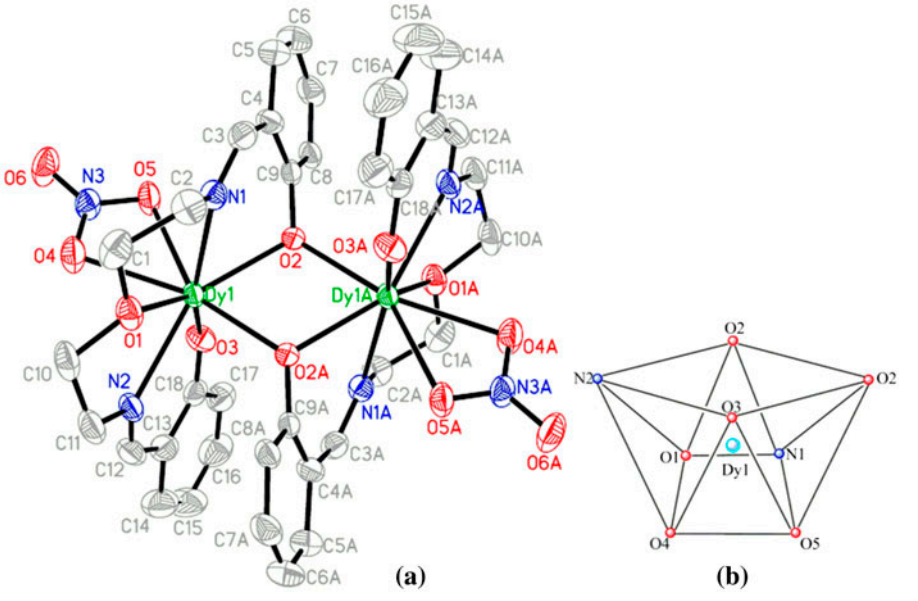

Figure 3. (a) The molecular structure of **2** in the crystal with displacement ellipsoids at 30% probability level; hydrogens are omitted for clarity. (b) Coordination polyhedron of Dy.

hypochromism of 57.7%. The hypochromisms observed for $\pi \rightarrow \pi^*$ transitions indicate strong binding of H_2L and complexes to DNA.

To compare quantitatively the affinity of H_2L and Ln(III) complexes to DNA, the intrinsic binding constants K_b of the two compounds to CT-DNA were determined by monitoring the changes of absorbance with increasing concentration of DNA. The intrinsic binding constants K_b of H_2L, **1** and **2** are $(5.30 \pm 0.10) \times 10^3\ M^{-1}$ ($R = 0.99$ for 16 points), $(4.13 \pm 0.08) \times 10^4\ M^{-1}$ ($R = 0.99$ for 16 points), $(5.63 \pm 0.08) \times 10^4\ M^{-1}$ ($R = 0.99$ for 16 points), respectively, from the decay of the absorbances. The K_b values obtained here are lower than those reported for classical intercalators (for ethidium bromide and [Ru(phen) DPPZ] whose binding constants have been found to be in the order of 10^6–$10^7\ M^{-1}$) [54–57]. It is clear that the hypochromism and K_b values are not enough evidence, but these results suggest an association of the compounds with CT-DNA and indicate that the binding strengths are in the order **2** > **1** > H_2L.

The affinity for DNA is stronger for Ln(III) complexes compared with H_2L. For this difference, we attributed two possible reasons. (i) The electrostatics of positively charged Ln^{3+} ions cause an interaction with polyanionic DNA. (ii) The charge transfer of coordinated H_2L, caused by coordination of Ln(III), results in reduction of charge density of the planar conjugated system; this change will lead to complexes binding to DNA more easily [58, 59].

3.3.2. Fluorescence spectroscopic studies. To further study the binding of the complexes with DNA, competitive binding experiments were carried out. Relative binding of H_2L and Ln(III) complexes to CT-DNA were studied by fluorescence spectra using ethidium bromide

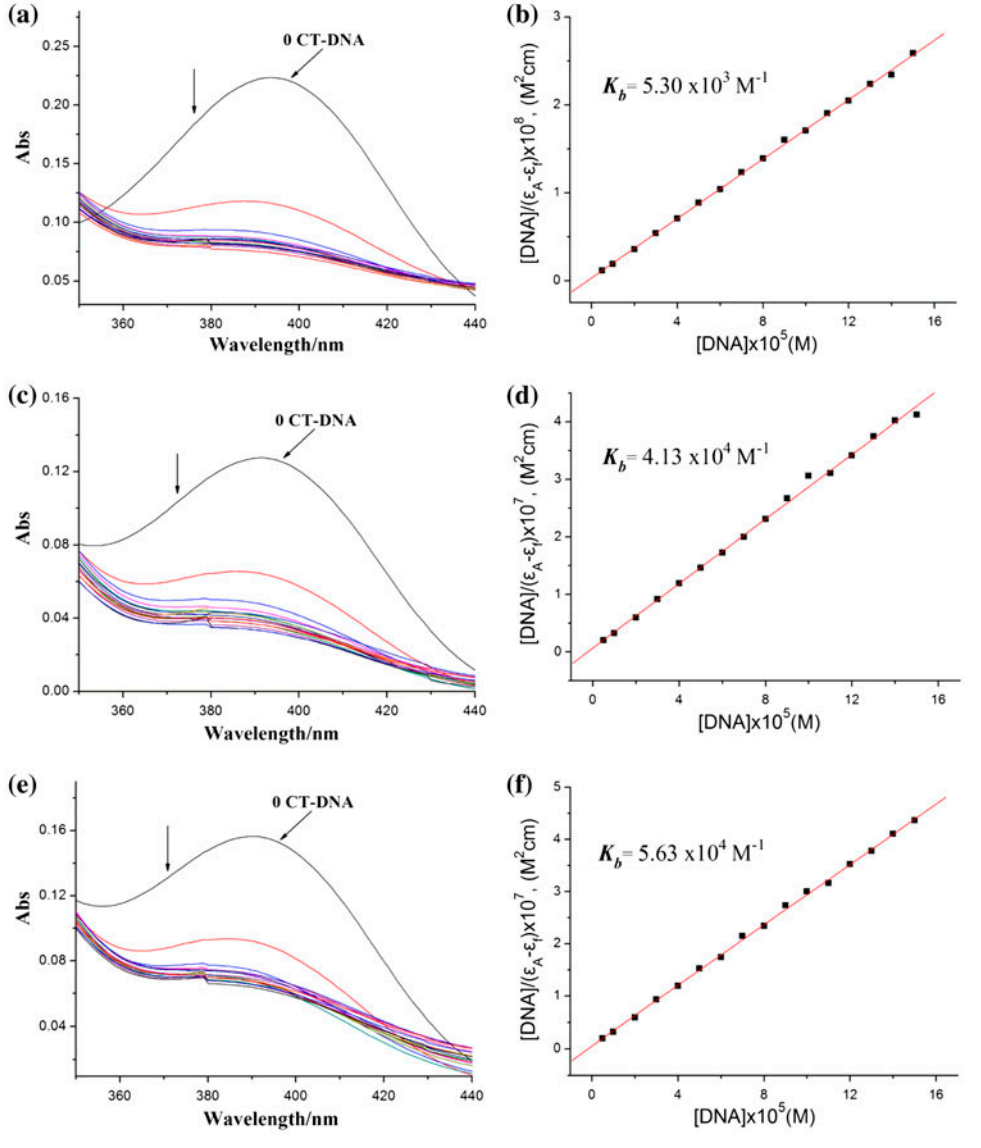

Figure 4. Electronic spectra of (a) H_2L, (c) **1**, (e) **2** in Tris–HCl buffer upon addition of CT-DNA. [Compound] = 3×10^{-5} M, [DNA] = 2.5×10^{-5} M. Arrow shows the emission intensity changes upon increasing DNA concentration. Plots of [DNA]/($\varepsilon_a - \varepsilon_f$) *vs.* [DNA] for the titration of (b) H_2L, (d) **1**, (f) **2** with CT-DNA.

(EB) bound CT-DNA solution in Tris–HCl/NaCl buffer (pH 7.2). As a typical indicator of intercalation, EB is a weakly fluorescent compound. But with DNA, emission intensity of EB is greatly enhanced because of its strong intercalation between adjacent DNA base pairs [37]. Measurement of the ability of a complex to affect the intensity of EB fluorescence in EB-DNA adduct allows determination of the affinity of the complex for DNA, whatever the binding mode may be. If a complex can displace EB from DNA, the fluorescence of the solu-

tion will be reduced due to the fact that free EB molecules are readily quenched by solvent water [60]. For H_2L and the Ln(III) complexes, no emission was observed either alone or in the presence of CT-DNA in the buffer. The fluorescence quenching of DNA-bound EB by H_2L, **1**, and **2** are shown in figure 5. The behavior of H_2L, **1**, and **2** are in agreement with the Stern–Volmer equation, which provides further evidence that the compounds bind to DNA. The K_{sv} values for H_2L, **1**, and **2** are $(0.35 \pm 0.010) \times 10^4$ ($R = 0.98$ for 21 points in the line

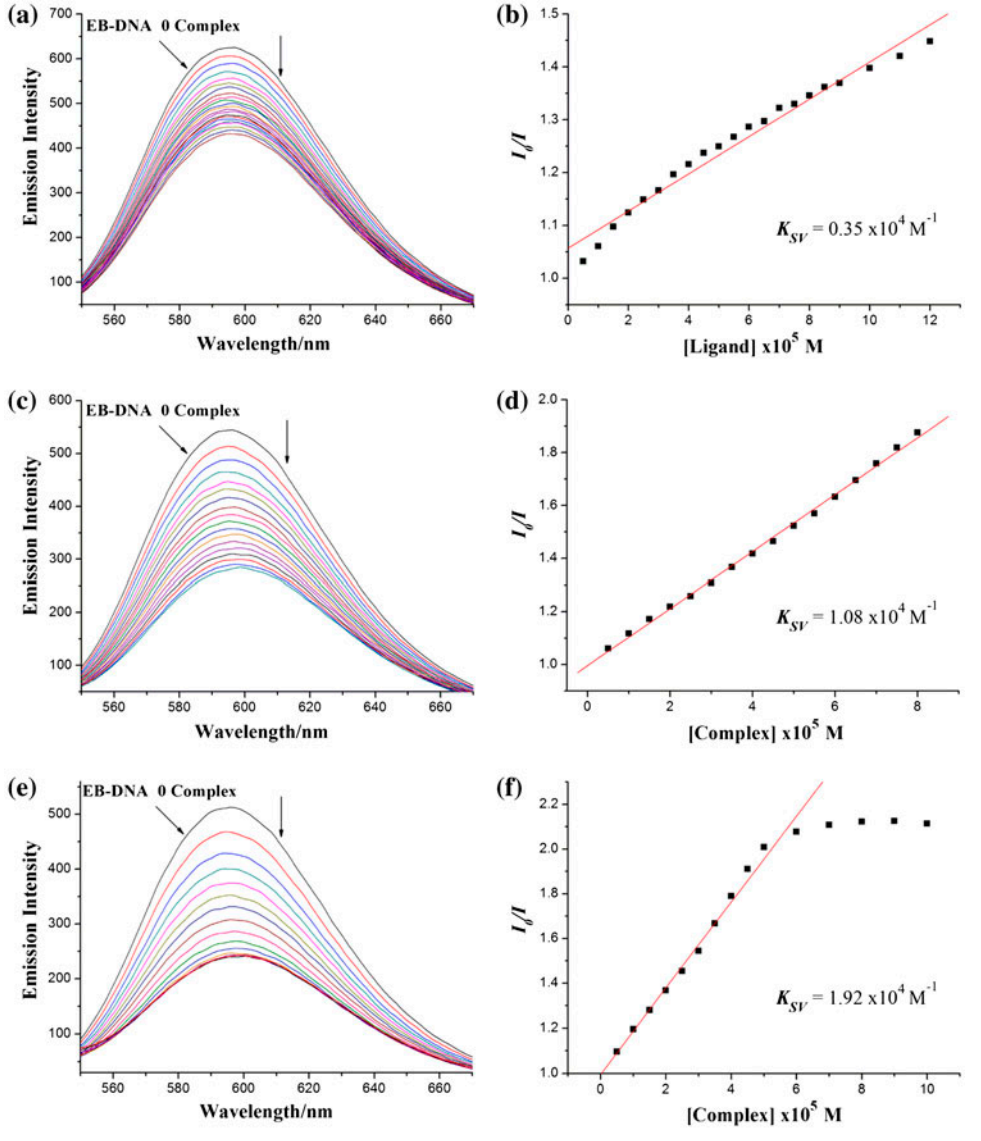

Figure 5. Emission spectra of EB bound to CT-DNA in the presence of (a) H_2L, (c) **1** and (e) **2**; [Compound] $= 3 \times 10^{-5}$ M; $\lambda_{ex} = 520$ nm. The arrows show the intensity changes upon increasing concentrations of the complexes. Fluorescence quenching curves of EB bound to CT-DNA by (b) H_2L, (d) **1** and (f) **2**. (Plots of I_0/I *vs.* [Complex].)

part), $(1.08 \pm 0.079) \times 10^4\ M^{-1}$ ($R = 0.99$ for 16 points), and $(1.92 \pm 0.094) \times 10^4\ M^{-1}$ ($R = 0.99$ for 11 points), respectively, reflecting the higher quenching efficiency of the complexes relative to that of H_2L. These results suggest DNA-binding of Ln(III) complexes (Ln = Gd, Dy) are stronger than that of H_2L. Such a trend is consistent with the previous absorption spectral results.

Figure 5 shows the plots of I_0/I *versus* [Component]. The data of K_{sv} are all at $10^4\ M^{-1}$ level for the ligand and its Ln(III) complexes, accordingly. In view of the strong interaction of EB with DNA with binding constant of EB $10^6\ M^{-1}$ level [56], we consider it impossible for the complexes to remove EB from DNA. Similar fluorescence quenching effect of EB bound to DNA has been observed for the addition of several groove-binding compounds, including netropsin and distamycin A [28, 60]. The observed results indicate that the complexes interact with DNA through the groove binding or intercalation, releasing some EB from the EB-DNA system [61–63].2

3.3.3. Viscosity titration measurements. Viscosity titration measurements were carried out to clarify the interaction modes between the investigated compounds and CT-DNA. Hydrodynamic measurements that are sensitive to changes in the length of DNA (i.e. viscosity and sedimentation) are regarded as the least ambiguous and the most critical tests of binding in solution in the absence of crystallographic structural data [64]. Classic intercalation involves insertion of a planar molecule between DNA base pairs, which results in a decrease in the DNA helical twist and lengthening of the DNA; the molecule will be in close proximity to the DNA base pairs as well [58, 59]. In contrast, molecule that binds exclusively in the DNA grooves by partial and/or non-classical intercalation typically cause less pronounced (positive or negative) or no change in DNA solution viscosity [65, 66].

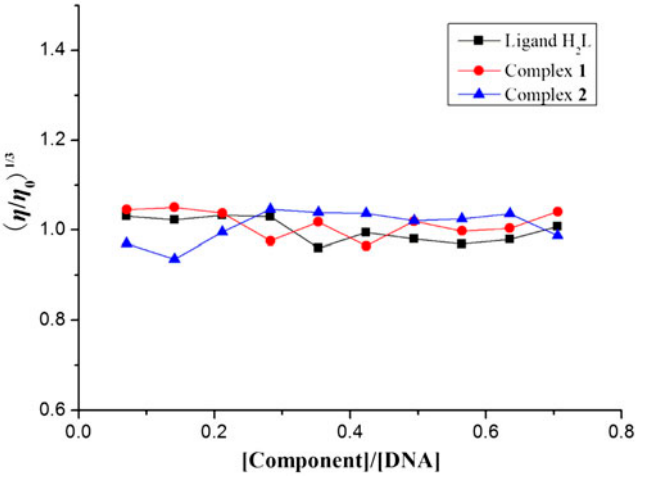

Figure 6. Effect of increasing amounts of Ln(III) complexes on the relative viscosity of CT-DNA at 25.0 ± 0.1 °C.

The effects of H_2L, **1**, and **2** on the viscosity of CT-DNA are shown in figure 6. Addition of the ligand and the two complexes cause no significant viscosity change, indicating that these compounds can bind to DNA by groove modes [65, 66].

3.4. *Antioxidant activities*

Generation of reactive oxygen species (ROS) is a normal process in the life of aerobic organisms. Free radical-induced DNA damage in humans is at biologically relevant levels, with approximately 10^4 DNA bases being oxidatively modified per cell per day. Oxidative damage to DNA has been suggested to contribute to aging and various diseases including cancer and chronic inflammation [67]. Since among all ROS, the hydroxyl (OH·) and superoxide radicals ($O_2^{-\cdot}$) are by far the most potent and therefore the most dangerous oxygen metabolites, elimination of these radicals is one of the major aims of antioxidant administration [68]. Consequently, in this article, H_2L, **1**, and **2** are studied for their antioxidant activities by comparing their scavenging effects on hydroxyl radical (OH·) and superoxide radical ($O_2^{-\cdot}$).

3.4.1. Hydroxyl radical scavenging activity. Figure 7 shows plots of hydroxyl radical scavenging effects (%) for the ligand, **1** and **2**. The values of IC_{50} of H_2L, **1**, and **2** for hydroxyl radical scavenging effects are $(7.1 \pm 0.1) \times 10^{-5}$ M^{-1}, $(6.59 \pm 0.09) \times 10^{-5}$ M^{-1}, $(3.66 \pm 0.07) \times 10^{-5}$ M^{-1}, respectively, with the order of **2** < **1** < H_2L. The hydroxyl radical scavenging effects of the Ln(III) complexes are much higher than that of H_2L. Moreover, we compared the abilities of one present compounds to scavenge hydroxyl radical (OH·) with those of well-known natural antioxidants mannitol and vitamin C using the same method as reported in a previous paper [69]. The 50% inhibitory concentration (IC_{50}) value of mannitol and vitamin C are 9.6×10^{-3} and 8.7×10^{-3} M^{-1}, respectively. The results

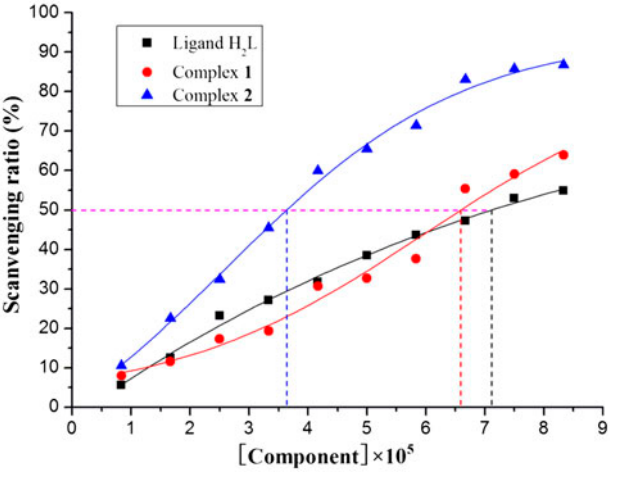

Figure 7. The inhibitory effect of H_2L and the Ln(III) complexes on OH· radicals; the suppression ratio increases with increasing concentration of the test compound.

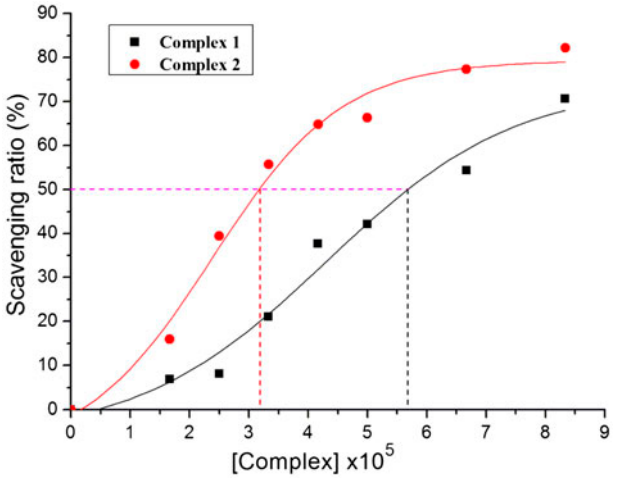

Figure 8. The inhibitory effect of the Ln(III) complexes on $O_2^{-\cdot}$ radicals; the suppression ratio increases with increasing concentration of the test compound.

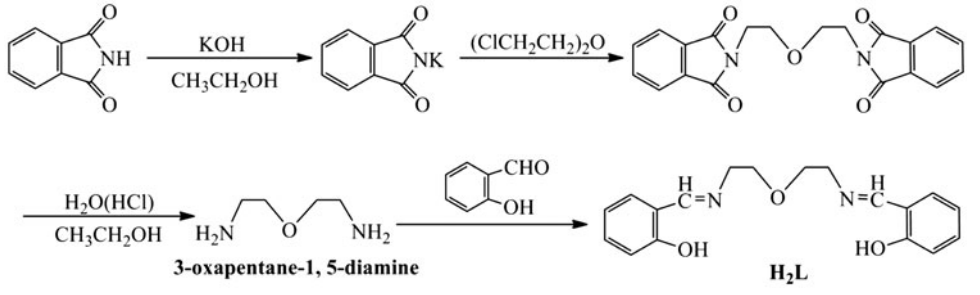

Scheme 1. Synthetic route of H_2L.

imply that **1** and **2** have ability to scavenge hydroxyl radical (OH·). Due to the observed IC_{50} values, the Ln(III) complexes (Ln = Gd, Dy) can be considered as potential drugs to eliminate the hydroxyl radical (OH·).

3.4.2. Superoxide radical scavenging activity. As another assay of antioxidant activity, superoxide radical ($O_2^{-\cdot}$) scavenging activity has been investigated. Both **1** and **2** have good superoxide radical scavenging activity. Complexes **1** and **2** show the IC_{50} value of $(5.7 \pm 0.1) \times 10^{-5}$ M^{-1} and $(3.19 \pm 0.09) \times 10^{-5}$ M^{-1}, indicating that they have scavenging activity for superoxide radical ($O_2^{-\cdot}$) (figure 8). The results indicate that **1** and **2** exhibit good superoxide radical scavenging activity and may be an inhibitor to scavenge superoxide radical ($O_2^{-\cdot}$) *in vivo*.

Table 4. Comparison of structural and biological properties of similar compounds.

Compounds	DNA-binding properties		Antioxidant properties		CS/CN
	$K_b/(M^{-1})$	$K_{SV}/(M^{-1})$	Hydroxyl radical $IC_{50}/(M)$	Superoxide radical $IC_{50}/(M)$	
$PrL(NO_3)(DMF)(H_2O)$[70]	9.34×10^4	2.14×10^4	6.14×10^{-5}	6.72×10^{-5}	mono/9
$Sm(L)(NO_3)(DMF)(H_2O)$[32]	1.19×10^5	2.01×10^4	5.58×10^{-5}	6.01×10^{-5}	mono/9
$[Eu(H_2L)_2(NO_3)_3]_n$[32]	4.22×10^4	1.83×10^4	3.39×10^{-5}	4.38×10^{-5}	poly/10
$GdL(NO_3)(DMF)(H_2O)$	4.13×10^4	1.08×10^4	6.59×10^{-5}	5.68×10^{-5}	mono/9
$Tb_2(L)_2(NO_3)_2$[32]	3.89×10^4	1.50×10^4	6.01×10^{-5}	3.39×10^{-5}	bi/8
$Dy_2L_2(NO_3)_2 \cdot 2H_2O$	5.63×10^4	1.92×10^4	3.66×10^{-5}	3.19×10^{-5}	bi/8
$Ho_2L_2(NO_3)_2 \cdot 2H_2O$[70]	1.59×10^4	1.92×10^4	3.95×10^{-5}	4.57×10^{-5}	bi/8
$Er_2(\mu\text{-}L)_2(NO_3)_2 \cdot 2H_2O$[71]	3.19×10^4	2.51×10^4	3.99×10^{-5}	5.19×10^{-5}	bi/8
$Yb_2(L)_2(NO_3) \cdot 2H_2O$[72]	3.17×10^4	1.48×10^4	3.35×10^{-5}	4.57×10^{-5}	bi/8
$Lu_2(L)_2(NO_3)_2$[27]	2.30×10^4	1.07×10^4	4.44×10^{-5}	4.06×10^{-5}	bi/8
$Y_2L_2(NO_3) \cdot H_2O$[28]	2.30×10^4	1.25×10^4	3.73×10^{-5}	4.23×10^{-5}	bi/8
Ligand	0.53×10^4	0.35×10^4	7.13×10^{-5}	–	–

Notes: Ligand – bis(N-salicylidene)-3-oxapentane-1,5-diamine; CS – crystal structure; CN – coordination number; K_b – intrinsic binding constant; K_{SV} – linear Stern–Volmer quenching constant; IC_{50} – The 50% inhibitory concentration; mono – mononuclear complex; bi – binuclear complex; poly – polynuclear complex.

4. Conclusion

Lanthanide (Gd(III) and Dy(III)) nitrate complexes of a pentadentate Schiff base ligand, bis (*N*-salicylidene)-3-oxapentane-1,5-diamine, have been synthesized and characterized. The crystal structures were determined by single-crystal X-ray diffraction. The DNA-binding properties of the ligand and Ln(III) complexes were investigated by spectra titration and viscosity measurements. The complexes bind to CT-DNA both via the groove binding mode, and the complexes have stronger binding affinity than H_2L. The Ln(III) complexes (Ln = Gd, Dy) exhibited antioxidant activities against OH· and $O_2^{-\cdot}$ radicals *in vitro*, and **2** is more effective than **1**.

We summarize our obtained compounds in table 4. Comparing the data of the compounds, we get the following conclusions. (i) The size of the rare earth ions might impact the structure of the complexes. The heavy rare earth ions form binuclear complexes, and the light rare earth ions form mononuclear or polynuclear complexes. This is mainly attributed to the "lanthanide contraction effect." (ii) The complexes have stronger binding affinity to DNA than the ligand. Differences in the structures of the complexes had no significant effect on the DNA-binding properties. (iii) The hydroxyl radical scavenging effects of complexes are higher than that of the ligand. The complexes exhibit good superoxide radical scavenging activity, but the ligand has no activity.

These findings indicate that the Ln(III) complexes have practical applications for the development of nucleic acid molecular probes and new therapeutic reagents for diseases on the molecular level. However, their pharmacodynamical, pharmacological, and toxicological properties should be further studied *in vivo*.

Supplementary material

Crystallographic data (excluding structure factors) for the structures reported in this article have been deposited with the Cambridge Crystallographic Data Center with reference

numbers CCDC 939873 and 939874. Copies of the data can be obtained, free of charge, on application to the CCDC, 12 Union Road, Cambridge CB2 1EZ, UK. Tel: +44 01223 762910; Fax: +44 01223 336033; E-mail: deposit@ccdc.cam.ac.uk or http://www.ccdc.cam.ac.uk.

Funding

The present research was supported by the National Natural Science Foundation of China [grant number 21367017]; the Fundamental Research Funds for the Gansu Province Universities [grant number 212086]; Natural Science Foundation of Gansu Province [grant number 1212RJZA037]; and 'Qing Lan' Talent Engineering Funds for Lanzhou Jiaotong University.

References

[1] F. Gao, H. Chao, F. Zhou, X. Chen, Y.F. Wei, L.N. Ji. *J. Inorg. Biochem.*, **102**, 1050 (2008).
[2] D.L. Arockiasamy, S. Radhika, R. Parthasarathi, B.U. Nair. *Eur. J. Med. Chem.*, **44**, 2044 (2009).
[3] F. Gao, X. Chen, J.Q. Wang, Y. Chen, H. Chao, L.N. Ji. *Inorg. Chem.*, **48**, 5599 (2009).
[4] Y.J. Liu, C.H. Zeng, H.L. Huang, L.X. He, F.H. Wu. *Eur. J. Med. Chem.*, **45**, 564 (2010).
[5] Z.M. Xu, S. Swavey. *Dalton Trans.*, **40**, 7319 (2011).
[6] M.J. Clarke. *Coord. Chem. Rev.*, **236**, 209 (2003).
[7] P. Tamil Selvi, H. Stoeckli-Evans, M. Palaniandavar. *J. Inorg. Biochem.*, **99**, 2110 (2005).
[8] K.E. Erkkila, D.T. Odom, J.K. Barton. *Chem. Rev.*, **99**, 2777 (1999).
[9] L.N. Ji, X.H. Zou, J.G. Lin. *Coord. Chem. Rev.*, **216/217**, 513 (2001).
[10] H.L. Wu, X.C. Huang, J.K. Yuan, F. Kou, F. Jia, B. Liu, K.T. Wang. *Eur. J. Med. Chem.*, **45**, 5324 (2010).
[11] P. Nagababu, J. Naveena lavanya latha, M. Rajesh, S. Satyanarayana. *J. Iran. Chem. Soc.*, **6**, 145 (2009).
[12] Z.H. Xu, X.W. Zhang, W.Q. Zhang, Y.H. Gao, Z.Z. Zeng. *Inorg. Chem. Commun.*, **14**, 1569 (2011).
[13] P. Kumar, B. Baidya, S.K. Chaturvedi, R.H. Khan, D. Manna, B. Mondal. *Inorg. Chim. Acta*, **376**, 264 (2011).
[14] B.M. Zeglis, V.C. Pierre, J.K. Barton. *Chem. Commun.*, **44**, 4565 (2007).
[15] S. Chattopadhyay, M.G.B. Drew, A. Ghosh. *Eur. J. Inorg. Chem.*, **10**, 1693 (2008).
[16] S.M. Abdallah, G.G. Mohamed, M.A. Zayed, M.S. El-Ela. *Spectrochim. Acta Part A: Mol. Biomol. Spectrosc.*, **73**, 833 (2009).
[17] K. Karaoglu, T. Baran, K. Serbest, M. Er, I. Degirmencioglu. *J. Mol. Struct.*, **922**, 39 (2009).
[18] J. Chakraborty, S. Thakurta, G. Pilet, R.F. Ziessel, L.J. Charbonnière, S. Mitra. *Eur. J. Inorg. Chem.*, **26**, 3993 (2009).
[19] W. Radecka-Paryzek, V. Patroniak, J. Lisowski. *Coord. Chem. Rev.*, **249**, 2156 (2005).
[20] P.A. Vigato, S. Tamburini. *Coord. Chem. Rev.*, **248**, 1717 (2004).
[21] E.N. Chygorin, O.V. Nesterova, J.A. Rusanova, V.N. Kokozay, V.V. Bon, R. Boča, A. Ozarowski. *Inorg. Chem.*, **51**, 386 (2012).
[22] S. Sasmal, S. Hazra, P. Kundu, S. Majumder, N. Aliaga-Alcalde, E. Ruiz, S. Mohanta. *Inorg. Chem.*, **49**, 9517 (2010).
[23] S. Liao, X.P. Yang, R.A. Jones. *Cryst. Growth Des.*, **12**, 970 (2012).
[24] B.D. Wang, Z.Y. Yang, T.R. Li. *Bioorg. Med. Chem.*, **14**, 6012 (2006).
[25] M. Marinić, I. Piantanida, G. Rusak, M. Žinić. *J. Inorg. Biochem.*, **100**, 288 (2006).
[26] Z.Y. Yang, B.D. Wang, Y.H. Li. *J. Organomet. Chem.*, **691**, 4159 (2006).
[27] G.L. Pan, Y.C. Bai, H. Wang, J. Kong, F.R. Shi, Y.H. Zhang, X.L. Wang, HL Wu. *Z. Naturforsch. B*, **68**, 257 (2013).
[28] H.L. Wu, G.L. Pan, Y.C. Bai, H. Wang, J. Kong, F.R. Shi, Y.H. Zhang, X.L. Wang. *J. Coord. Chem.*, **66**, 2634 (2013).
[29] S. Satyanarayana, J.C. Dabrowiak, J.B. Chaires. *Biochemistry*, **32**, 2573 (1993).
[30] J. Marmur. *J. Mol. Biol.*, **3**, 208 (1961).
[31] S.M. Nelson, C.V. Knox. *J. Chem. Soc., Dalton Trans.*, 2525 (1983).
[32] H.L. Wu, G.L. Pan, Y.C. Bai, Y.H. Zhang, H. Wang, F.R. Shi, X.L. Wang, J. Kong. *J. Photochem. Photobiol. B*, **135**, 33 (2014).
[33] Bruker. *SMART, SAINT and SADABS*, Bruker AXS Inc, Madison, WI (2000).
[34] G.M. Sheldrick. *SHELXTL*, Siemens Analytical X-ray Instruments Inc, Madison, WI (1996).
[35] A.M. Pyle, J.P. Rehmann, R. Meshoyrer, C.V. Kumar, N.J. Turro, J.K. Barton. *J. Am. Chem. Soc.*, **111**, 3051 (1989).
[36] A. Wolfe, G.H. Shimer Jr. T. Meehan. *Biochemistry*, **26**, 6392 (1987).
[37] B.C. Baguley, M. Le Bret. *Biochemistry*, **23**, 937 (1984).
[38] J.R. Lakowicz, G. Weber. *Biochemistry*, **12**, 4161 (1973).

[39] C.P. Tan, J. Liu, L.M. Chen, S. Shi, L.N. Ji. *J. Inorg. Biochem.*, **102**, 1644 (2008).
[40] C.C. Winterbourn. *Biochem. J.*, **198**, 125 (1981).
[41] C.C. Winterbourn. *Biochem. J.*, **182**, 625 (1979).
[42] Z.Y. Guo, R.E. Xing, S. Liu, H.H. Yu, P.B. Wang, C.P. Li, P.C. Li. *Bioorg. Med. Chem. Lett.*, **15**, 4600 (2005).
[43] C. Beauchamp, I. Fridovich. *Anal. Biochem.*, **44**, 276 (1971).
[44] Q.H. Luo, Q. Lu, A.B. Dai, L.G. Huang. *J. Inorg. Biochem.*, **51**, 655 (1993).
[45] W.K. Dong, G. Wang, S.S. Gong, J.F. Tong, Y.X. Sun, X.H. Gao. *Transition Met. Chem.*, **37**, 271 (2012).
[46] H.L. Wu, F. Jia, F. Kou, B. Liu, J.K. Yuan, Y. Bai. *J. Coord. Chem.*, **64**, 3454 (2011).
[47] K. Nakamoto. *Infrared and Raman Spectra of Inorganic and Coordination Compounds*, 4th Edn, p. 284, Wiley, New York (1986).
[48] L. Casella, M. Gullotti, A. Pintar, L. Messori, A. Rockenbauer, M. Gyor. *Inorg. Chem.*, **26**, 1031 (1987).
[49] Y. Huang, B. Yan, M. Shao. *Solid State Sci.*, **10**, 90 (2008).
[50] S.C. Manna, E. Zangrando, A. Bencini, C. Benelli, N.R. Chaudhuri. *Inorg. Chem.*, **45**, 9114 (2006).
[51] C. Qin, X.L. Wang, E.B. Wang, L. Xu. *Inorg. Chim. Acta*, **359**, 417 (2006).
[52] W.K. Dong, Y.X. Sun, L. Li, S.T. Zhang, L. Wang, X.Y. Dong, X.H. Gao. *J. Coord. Chem.*, **65**, 2332 (2012).
[53] J.K. Barton, A.T. Danishefsky, J.M. Goldberg. *J. Am. Chem. Soc.*, **106**, 2172 (1984).
[54] M. Cory, D.D. McKee, J. Kagan, D.W. Henry, J.A. Miller. *J. Am. Chem. Soc.*, **107**, 2528 (1985).
[55] M.J. Waring. *J. Mol. Biol.*, **13**, 269 (1965).
[56] V.G. Vaidyanathan, B.U. Nair. *J. Inorg. Biochem.*, **94**, 121 (2003).
[57] R. Vijayalakshmi, M. Kanthimathi, V. Subramanian, B.U. Nair. *Biochim. Biophys. Acta*, **1475**, 157 (2000).
[58] H.L. Wu, J.K. Yuan, Y. Bai, G.L. Pan, H. Wang, J. Kong, X.Y. Fan, H.M. Liu. *Dalton Trans.*, **41**, 8829 (2012).
[59] H.L. Wu, J.K. Yuan, Y. Bai, G.L. Pan, H. Wang, X.B. Shu. *J. Photochem. Photobiol. B*, **107**, 65 (2012).
[60] J.-B. Lepecq, C. Paoletti. *J. Mol. Biol.*, **27**, 87 (1967).
[61] S.M. Nelson, L.R. Ferguson, W.A. Denny. *Mutat. Res.*, **623**, 24 (2007).
[62] D.L. Boger, B.E. Fink, S.R. Brunette, W.C. Tse, M.P. Hedrick. *J. Am. Chem. Soc.*, **123**, 5878 (2001).
[63] Z.Q. Liu, M. Jiang, Y.T. Li, Z.Y. Wu, J.X. Yang. *Inorg. Chim. Acta*, **362**, 1253 (2009).
[64] D.S. Sigman, A. Mazumder, D.M. Perrin. *Chem. Rev.*, **93**, 2295 (1993).
[65] B.D. Wang, Z.Y. Yang, P. Crewdson, D.Q. Wang. *J. Inorg. Biochem.*, **101**, 1492 (2007).
[66] J.M. Kelly, A.B. Tossi, D.J. McConnell, C. OhUigin. *Nucleic Acids Res.*, **13**, 6017 (1985).
[67] K. Tsai, T.G. Hsu, K.M. Hsu, H. Cheng, T.Y. Liu, C.F. Hsu, C.W. Kong. *Free Radical Biol. Med.*, **31**, 1465 (2001).
[68] N. Udilova, A.V. Kozlov, W. Bieberschulte, K. Frei, K. Ehrenberger, H. Nohl. *Biochem. Pharmacol.*, **65**, 59 (2003).
[69] T.R. Li, Z.Y. Yang, B.D. Wang, D.D. Qin. *Eur. J. Med. Chem.*, **43**, 1688 (2008).
[70] H.L. Wu, Y.C. Bai, Y.H. Zhang, G.L. Pan, J. Kong, F.R. Shi, X.L. Wang. *Z. Anorg. Allg. Chem.*, **640**, 2062 (2014).
[71] H.L. Wu, G.L. Pan, Y.C. Bai, H. Wang, J. Kong, F.R. Shi, Y.H. Zhang, X.L. Wang. *J. Chem. Res.*, **38**, 197 (2014).
[72] H.L. Wu, G.L. Pan, Y.C. Bai, H. Wang, J. Kong, F.R. Shi, Y.H. Zhang, X.L. Wang. *Res. Chem. Intermed*. doi: 10.1007/s11164-013-1440-5.